Evidence for Subsurface Ordering of Oxygen Vacancies on the Reduced $CeO_2(111)$ Surface Using Density-Functional and Statistical Calculations

Gustavo E. Murgida

Centro Atómico Constituyentes, GIyA, CNEA, San Martín, Buenos Aires, Argentina and Consejo Nacional de Investigaciones Científicas y Técnicas, C1033AAJ, Buenos Aires, Argentina

M. Verónica Ganduglia-Pirovano*

Instituto de Catálisis y Petroleoquímica of the Consejo Superior de Investigaciones Científicas, 28049 Madrid, Spain

(Received 3 August 2012; revised manuscript received 1 April 2013; published 11 June 2013)

Oxygen vacancies on ceria (CeO_2) surfaces play a crucial role in catalytic applications, yet whether vacancies are at surface or subsurface sites on reduced $CeO_2(111)$, and whether vacancies agglomerate or repel each other, is still under discussion, with few and inconsistent experimental results. By combining density-functional theory (DFT) in the DFT + U (U is an effective onsite Coulomb interaction parameter) approach and statistical thermodynamics, we show that the energetically most stable near-surface oxygen vacancy structures for a broad range of vacancy concentrations, Θ ($\frac{1}{16} \leq \Theta \leq 1$ monolayer) have all vacancies at subsurface oxygen sites and predict that the thermodynamically stable phase for a wide range of reducing conditions is a (2×2) ordered subsurface vacancy structure ($\Theta = \frac{1}{4}$). Vacancy-induced lattice relaxations effects are crucial for the interpretation of the repulsive interactions, which are at the basis of the vacancy spacing in the (2×2) structure. The findings provide theoretical data to support the interpretation of the most recent experiments, bringing us closer to solving the debate.

DOI: 10.1103/PhysRevLett.110.246101 PACS numbers: 82.65.+r, 68.35.Dv, 71.15.Mb

Materials based on ceria (CeO_2) are extremely important in catalysts for automotive exhaust treatment and the hydrogen economy [1–4] as well as in many other applications, such as gate oxides in microelectronic devices, materials for nonvolatile resistive random access memories, oxide-ion conductors in solid-oxide fuel cells [5], and sensors, with the reducibility of the system being crucial to its functionality in such applications. For ceria, in common with other reducible oxides (see, e.g., Refs. [6,7]), the in-depth understanding and control of the type, density, and distribution of oxygen vacancies provide a means to influence the electronic structure and to tailor the systems' functionality. This has been the driving force for pursuing experimental and theoretical research on low-index reduced ceria surfaces [8–18]. Despite these efforts, to date, for the (111) surface, there is a notable lack of consistency between experimental results on whether oxygen vacancies are more stable at surface or subsurface sites and on whether they attract or repel. [8,9,16] In the STM study by Esch *et al.* [8], equally distributed isolated surface and subsurface vacancies, and predominantly linear along with triangular arrangements of first-nearest-neighbor surface vacancies, consecutively appeared as annealing proceeded. In contrast, in the atomic force microscopy (AFM) study by Torbruegge *et al.* [9], a local ordering of third-nearest-neighbor subsurface vacancies forming a (2×2) pattern was found. Moreover, in a more recent STM study on ultrathin films of $CeO_2(111)$ by Grinter *et al.* [16], a high density of subsurface vacancies, which for the most part formed pairs of third- and second-nearest-neighbor vacancies, was observed. The theoretical understanding of the structures of near-surface oxygen vacancies beyond the case of isolated vacancies [11–14,18–21] is very shallow. This is in part due to the existence of multiple local minima with respect to the sites on which the excess electrons, driving the $Ce^{4+} \rightarrow Ce^{3+}$ reduction, localize [11,12,17]. As yet, studies of vacancy aggregates are relatively scarce and limited to surface vacancies [13,14,18]; Conesa [13] found their interaction to be repulsive; however, in a more recent study by Amrute *et al.* [18], a slightly attractive interaction is found, consistent with the STM study by Esch *et al.* [8].

In this Letter we consider different vacancy structures—including surface and subsurface sites—and show that for a broad range of vacancy concentrations, Θ ($\frac{1}{16} \leq \Theta \leq 1$ ML), the most stable structures are where all vacancies are subsurface and also that these vacancies tend to separate up to a distance equal to twice the (1×1) surface lattice parameter, i.e., the third-nearest-neighbor distance in the oxygen layer. We produce firm computational evidence that the thermodynamically stable phase under a wide range of reducing conditions is a (2×2) ordered subsurface vacancy structure ($\Theta = \frac{1}{4}$), while vacancies form third-nearest-neighbor pairs at a lower vacancy concentration ($\Theta = \frac{1}{8}$) and thus provide support for the interpretation of the most recent experimental results [9,16]. The distance between vacancies is explained in terms of vacancy-induced lattice relaxation effects, which are linked to the excess-charge localization phenomena.

We apply the spin-polarized density-functional theory (DFT) in the DFT + U approach (where U is a Hubbard-like term describing the onsite Coulomb interactions) with the PBE (Perdew-Burke-Ernzerhof) functional [22] to partially reduced $CeO_2(111)$. The Kohn-Sham equations were solved using the projected augmented wave (PAW) method, as implemented in the Vienna *ab initio* simulation package (VASP) [23]. For Ce and O atoms, the $(5s, 5p, 6s, 4f, 5d)$ and $(2s, 2p)$ states, respectively, were treated as valence with a plane-wave cutoff energy of 400 eV. In the DFT + U calculations, the U_{eff} value [24] of 4.50 eV was used [20,25]. The $CeO_2(111)$ surface was modeled using a supercell containing a slab of nine atomic layers [Fig. 1(a)] with calculated CeO_2 bulk equilibrium lattice constant (5.485 Å) out of which six were allowed to relax with the surface unit cell kept fixed during geometry optimization. The reduced surface with only subsurface, mixed surface/subsurface, or only surface vacancies was studied for a wide range of vacancy concentrations, $\Theta = \frac{1}{16}, \frac{1}{8}, \frac{1}{4}, \frac{1}{2}, \frac{3}{4}$, and 1 monolayer (ML) with a (4×4), (2×2), and (1×1) surface periodicity and a $(1 \times 1 \times 1)$, $(3 \times 3 \times 1)$, and $(6 \times 6 \times 1)$ Monkhorst-Pack grid, respectively. $\Theta = N_v/N$, where N_v and N are the actual number of surface plus subsurface vacancies in the supercell and the number of atoms in a nonreduced oxygen layer within that cell, respectively. In order to identify the most stable structure at a given concentration, different possible combinations of the locations of both the vacancies and the associated Ce^{3+} ions were considered. The excess electrons do remain fully localized on Ce ions as the vacancy concentration increases from $\frac{1}{16}$ to 1 ML (see Supplemental Material [26], Fig. S8). In the construction of the models, preference was given to those for which vacancies were bound to Ce^{4+}, and the Ce^{3+} were next-nearest neighbor to the vacancies in accordance with recent literature [11,12,17] and rather in the outermost cerium layer. In addition, the distances between the Ce^{3+} ions were maximized. Notwithstanding these preferences, selected alternative configurations were also considered and are briefly mentioned later. We limit the discussion to high-spin states because the difference between these states and any other spin state is less than 0.01 eV. In total, 33 vacancy structures were investigated (see Supplemental Material [26]). Hereafter, the alike structures with respect to the vacancy location, i.e., subsurface, mixed surface and subsurface, or surface, are alphabetically labeled according to increasing energy. Thus, for a given vacancy concentration (Θ), $\Theta(a)_{ss}$, $\Theta(a)_{s\text{-}ss}$, and $\Theta(a)_s$ are the most stable structures of each type.

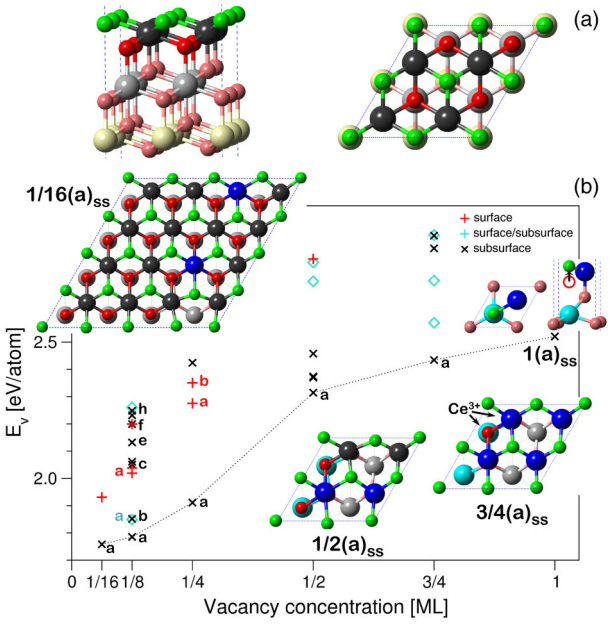

FIG. 1 (color online). (a) Structural model of the clean CeO_2 surface with (2×2) periodicity. O (Ce) atoms are represented by small (large) balls. (b) The averaged vacancy formation energy (E_v, with respect to $\frac{1}{2}O_2$ in eV/atom). Labels for selected structures are indicated (see text). The most stable $\Theta(a)_{ss}$ structures are shown (only the first five atomic layers are displayed); see also Figs. 2 [$\frac{1}{4}(a)_{ss}$] and 3 [$\frac{1}{8}(a)_{ss}$]. Ce^{3+} ions in the second atomic layer are represented darker than those in the fifth one. The $1(a)_{ss}$ structure corresponds to the $CeO_2(111)$ surface for which the terminating surface O atoms were removed. In the optimized structure, initially subsurface O atoms strongly relax outward leaving a vacant O layer behind, while becoming surface O atoms, and hence are represented as such.

The averaged vacancy formation energy, E_v, for all structures shows a clear trend [Fig. 1(b)]: for the whole range of vacancy concentrations ($\frac{1}{16} \leq \Theta \leq 1$ ML), $(a)_{ss} < (a)_{s\text{-}ss} < (a)_s$, i.e., the most stable structures consist of only subsurface vacancies. E_v for the $\Theta(a)_{ss}$ structures exhibits a sigmoidlike behavior, which will be examined in more detail later. For initial high-surface vacancy concentrations ($\Theta \geq \frac{3}{4}$ ML), there are significant lattice relaxations with large outward displacements of up to ~1.7 Å of subsurface oxygen atoms in the third atomic layer, so that they become surface ones, i.e., surface vacancies are unstable [cf. $1(a)_{ss}$ in Fig. 1(b)]. The subsurface preference at deep reduction levels has also been assessed using DFT with the HSE06 hybrid functional [27] (see Supplemental Material [26], Table S2).

For obtaining a theoretical prediction of the surface structure and composition in thermal equilibrium with an O_2 environment under reducing conditions (UHV and high temperatures) and with the bulk, we combine the DFT + U total energy calculations with statistical thermodynamics [28]. In the present study we are interested in the relative stability of the reduced ceria surfaces. To determine the stable structure at a given temperature and pressure, we calculate the change in the surface free energy, $\Delta\gamma$, as $\Delta\gamma(T, p, \Theta) = N_v/A[E_v(\Theta) + \Delta\mu_O(T, p)]$ [29]. N_v, A, and $\Delta\mu_O(T, p) = \frac{1}{2}[\mu_{O_2}(T, p) - E_{O_2}]$ are, respectively, the number of vacancies, the area of the surface unit cell, and the oxygen chemical potential where the total energy of an isolated molecule at $T = 0$ K is taken as the reference state. Figure 2 shows the results where $\Delta\gamma$ is displayed as a function of $\Delta\mu_O$ for the most stable structure at each

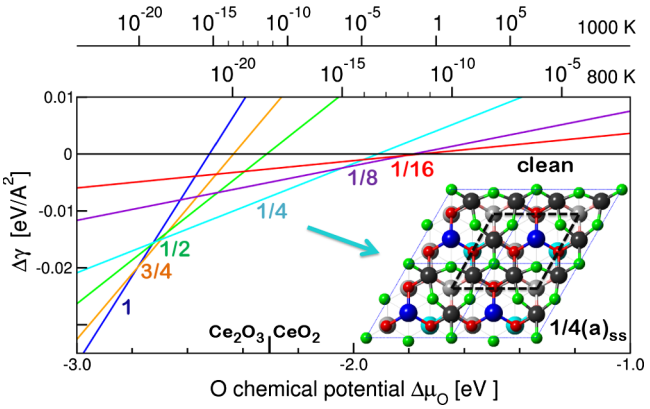

FIG. 2 (color online). Surface free energy change $\Delta\gamma$ as a function of the oxygen chemical potential $\Delta\mu_O$ for different vacancy concentrations. In the top x axis, $\Delta\mu_O(T, p)$ has been translated into a pressure scale (in atmospheres) assuming ideal gas behavior and using tabulated values [35] for the enthalpy and entropy at $T = 800$ and 1000 K. The dashed lines in the $\frac{1}{4}(a)_{ss}$ structure show the (2×2) local arrangement of subsurface vacancies.

vacancy concentration, i.e., $\Theta(a)_{ss}$. There is clearly one vacancy structure which is stable under a wide range of reducing conditions: the $\frac{1}{4}(a)_{ss}$ with subsurface vacancies forming a (2×2) pattern with all vacancies being third nearest neighbors in the oxygen layer. Here, it is important to mention that the PBE gradient approximation tendency to overestimate binding energies means that the oxygen chemical potential could be shifted by up to 0.5 eV [22]. Hence, the absolute pressures might be in error by 2 to 3 orders of magnitude. Nevertheless, the general stability trend is valid. Furthermore, we have also computed the configurational entropy contributions per unit area to $\Delta\gamma$ in the 0–1300 K temperature range using the standard equation $TS/A = -kT/a_{(1\times1)}[\Theta \ln(\Theta) + (1 - \Theta)\ln(1 - \Theta)]$, where $a_{(1\times1)}$ is the area of the (1×1) surface unit cell, and Θ is the defect concentration. In all cases, the configurational entropy contribution stays below 6 meV/Å^2 (see Supplemental Material [26], Sec. S3), and its inclusion does not change any of the conclusions drawn when the Gibbs free energies of the solid components are equated to the calculated DFT total energies evaluated at $T = 0$ K. Taking this into account, we notice a gratifying agreement between theory and the interpretation of a recent AFM experiment, where the (2×2) subsurface vacancy local ordering on the slighltly reduced $CeO_2(111)$ surface was observed [9]. According to the AFM experiment, the dominant type of defects on defective terraces on the surface are subsurface oxygen vacancies. Using models for surface segregation applied to the vacancies, namely, the simplest Langmuir-McLean (LM) model which assumes they are noninteracting and the more realistic Fowler-Guggenheim (FG) one in which an interaction is allowed [30], we calculated the percentage of surface vacancies in thermodynamic equilibrium at a given temperature. For instance, at 300 K, 0.12% of isolated defects ($\Theta = \frac{1}{16}$ ML) would occupy surface sites, and at 1000 K is 12%. As Θ increases, for instance at $\Theta = \frac{1}{4}$ ML and 1000 K, 7.8% of the defects would be at the surface according to the FG model (cf. 17.4% according to LM; see Supplemental Material [26], Fig. S11). The lower segregation is indicative of repulsive interactions between the vacancies. The near-surface region will be further reduced in response to increasing reducing conditions. The calculated value of the oxygen chemical potential below which bulk Ce_2O_3 oxide is thermodynamically more stable than bulk CeO_2 is $\Delta\mu_O < -2.30$ eV (cf. Fig. 2), but PBE + U(4.5 eV) underestimates the reaction energy of reduction $2CeO_2 \rightarrow Ce_2O_3 + \frac{1}{2}O_2$ by more than 1 eV [31]. Hence, the reduction that starts at the near-surface region may initiate the conversion to the lower bulk oxide, and the $1(a)_{ss}$ structure could represent a precursor to the phase transition. The similarity between the two outermost layers of the $1(a)_{ss}$ structure and those of the $Ce_2O_3(0001)$ surface was already pointed out [15]. If one is to overlay the corresponding surface unit cells, both surface areas overlap almost commensurately, with the calculated surface lattice vectors deviating by barely less than 0.04 Å [cf. 3.879 and 3.915 Å for (1×1) $CeO_2(111)$ and $Ce_2O_3(0001)$, respectively].

To rationalize why subsurface vacancies do not agglomerate but leave some space between them with a preferred spacing (7.76 Å) equal to twice the (1×1) surface lattice parameter, we investigate the extent to which the distance between vacancies forming pairs influences their formation energy. We calculate the (nonaveraged) energy for the formation of each vacancy upon O removal in successive steps, $\tilde{E}_v$, from the isolated vacancy [$\frac{1}{16}(a)_{ss}$] to vacancy pairs ($\Theta = \frac{1}{8}$) with varying vacancy separation, namely, 1, $\sqrt{3}$, and 2 times the closest possible distance between vacancies (cf. Fig. 3). Figure 3 shows the $\tilde{E}_v$ energy profile that includes both unrelaxed and fully relaxed geometries. The energies of formation of second vacancies are referred to the fully relaxed isolated vacancy structure. Thus, the unrelaxed geometries for the new vacancy correspond to the relaxed $\frac{1}{16}(a)_{ss}$ structure with one additional vacancy that was not allowed for further relaxation.

For an isolated subsurface vacancy, substantial lattice relaxations have been experimentally observed [8,9] and calculated [11,20]. The Ce atoms that are first neighbors to the vacancy move away from the vacant site, and the O atoms that are second neighbors to the defect move toward the vacant site. In addition, three surface O atoms are lifted by ~0.2 Å [9]. These relaxation effects are crucial to the localization of the two excess electrons following the vacancy formation [11], and the associated energy gain is quite substantial (~2.2 eV, cf. Fig. 3). Furthermore, we find that starting from the relaxed isolated vacancy structure, the energy required to create an additional unrelaxed subsurface vacancy forming a vacancy pair (cf. Fig. 3) remains approximately constant (within ~0.1 eV) as the distance between vacancies varies from 1 to 2 times the (1×1) surface lattice parameter and is

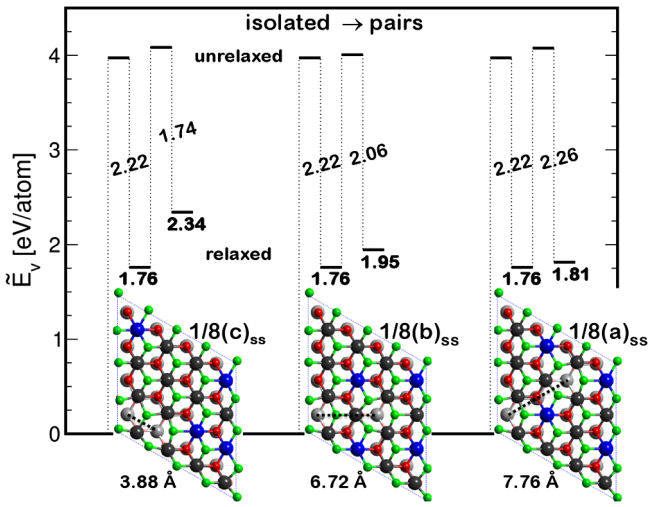

FIG. 3 (color online). Energy profile for the gradual removal of O atoms: from the isolated vacancy [$\frac{1}{16}(a)_{ss}$] to vacancy pairs with varying vacancy separation. Shown are the values for the unrelaxed and relaxed geometries and the relaxation contributions to the latter (see text).

slightly larger than that to create the first unrelaxed vacancy (by up to ~0.1 eV). For these (unrelaxed) structures, two additional excess electrons are equally shared by the four nearest-neighbor Ce cations to the new vacancy. The energy gain if further structural relaxations are allowed, which result in the localization of those two extra electrons in next-nearest- neighbor sites to the new vacancy, however, does depend on the distance between vacancies (cf. Fig. 3); it is ~1.7, 2.1, and 2.3 eV for vacancies on first, second, and third oxygen neighbor sites, respectively. The latter relaxation energy contribution approximately equals that for an isolated vacancy (~2.2 eV). A close inspection of the calculated structures revealed that the atomic displacements due to the first vacancy formation are, to some extent, counteracted by second vacancies, resulting in a net increase in the formation energy of additional vacancies as compared to isolated ones (cf. Fig. 3). These effects are predominantly large for extra vacancies on first oxygen neighbor sites and decrease with increasing vacancy separation. Consequently, after the initial vacancy formation, the most stable pair must consist of third-nearest-neighbor vacancies [$\frac{1}{8}(a)_{ss}$] rather than second [$\frac{1}{8}(b)_{ss}$], and certainly not first neighbor [$\frac{1}{8}(c)_{ss}$], which is exactly what Grinter *et al.* observed [16]. With respect to stability, we can compare [$2 \times \frac{1}{16}(a)_{ss}$] with [$\frac{1}{8}(c)_{ss}$ + $CeO_2(111)$], [$\frac{1}{8}(b)_{ss}$ + $CeO_2(111)$], and [$\frac{1}{8}(a)_{ss}$ + $CeO_2(111)$]; two subsurface vacancies, being first, second, or third nearest neighbors, have a repulsive interaction energy of 0.58, 0.19, and 0.05 eV, respectively. In other words, a subsurface vacancy repels vacancies from its nearest and next-nearest neighbor shells. This indicates that upon increasing the vacancy concentration, the formation of structures with all vacancies being third nearest neighbors, and thus having a negligible repulsion between them, must be preferred, which is just the case of the (2×2) vacancy phase [$\frac{1}{4}(a)_{ss}$] observed in the experiment of Torbruegge *et al.* [9].

Turning to the averaged defect formation energies [Fig. 1(b)], we note that the values for an isolated vacancy [1.76 eV, $\frac{1}{16}(a)_{ss}$] and for a third-nearest-neighbor vacancy pair [1.79 eV, $\frac{1}{8}(a)_{ss}$] are very similar, whereas that for the (2×2) structure with the same vacancy spacing is slightly larger [1.91 eV, $\frac{1}{4}(a)_{ss}$], giving rise to the smooth increase of the E_v curve for the $\Theta(a)_{ss}$ structures mentioned above. In all of these three structures, all vacancies have two Ce^{3+} ions in next-nearest-neighbor cation sites, but in the two former ones, they are located in the energetically preferred outermost cerium layer, whereas for the $\frac{1}{4}(a)_{ss}$ structure this is no longer possible; one Ce^{3+} is in a deeper (fifth) atomic layer. Furthermore, for $\Theta \geq \frac{1}{2}$, vacancies are in nearest-neighbor positions in the oxygen layer, and localization of excess electrons in energetically much less favored nearest-neighbor cation sites is also unavoidable; hence, the "jump" in the E_v values for the $\Theta(a)_{ss}$ structures.

As earlier indicated, we selectively considered alternative structures to those resulting from minimizing the number of Ce^{3+} in nearest-neighbor cation sites and having them preferably in the outermost cerium layer. Electron hopping between Ce sites can take place via a phonon-assisted mechanism [32] and is thermally activated (0.4–0.5 eV [33]). The $\frac{1}{8}(f)_{ss}$, $(g)_{ss}$, and $(h)_{ss}$ structures [cf. Fig. 1(b)] with third-nearest-neighbor vacancies having two Ce^{3+} ions in nearest-neighbor cation sites in the outermost cerium layer (see Supplemental Material [26]) are by 0.4–0.5 eV less stable than the comparable $\frac{1}{8}(a)_{ss}$ structure (Fig. 3) with Ce^{3+} ions in next-nearest neighbor sites. Similarly, the preference for Ce^{3+} ions in next-nearest neighbor sites to the defect is found for structures with second- and first-nearest-neighbor vacancies, namely, the $\frac{1}{8}(b)_{ss}$ [by 0.2 eV, cf. $\frac{1}{8}(d)_{ss}$] and $\frac{1}{8}(c)_{ss}$ [by 0.1 eV, cf. $\frac{1}{8}(e)_{ss}$] structures, respectively. Furthermore, even though the outermost cerium layer is generally the energetically preferred location of the Ce^{3+} ions, they would rather be in deeper layers than next to a vacancy. For instance, the $\frac{1}{4}(a)_s$ surface vacancy structure with both Ce^{3+} ions in next-nearest neighbor cation sites, one in the second and the other in the fifth atomic layer, is by ~0.1 eV more stable than the $\frac{1}{4}(b)_s$ structure with the Ce^{3+} on a pair of nearest and next-nearest neighbor cation sites in the outermost cerium layer. It appears clear that the preference for Ce^{3+} ions in sites not adjacent to the defect, as predicted for isolated vacancies [11,12,17] remains for all types of vacancy aggregates and concentrations, as much as possible.

In summary, DFT + U calculations in combination with statistical thermodynamics provide crucial insight into the thermodynamically stable near-surface oxygen vacancy structures on $CeO_2(111)$. We predict that for a wide range of reducing conditions, the stable phase is a (2×2) ordered subsurface vacancy structure ($\Theta = \frac{1}{4}$), with all

vacancies being third nearest neighbors in the oxygen layer. Vacancy ordering starts from isolated subsurface oxygen vacancies ($\Theta = \frac{1}{16}$), forming third-nearest-neighbor pairs with increasing vacancy concentration ($\Theta = \frac{1}{8}$). Our findings provide both support for the interpretation of the most recent experimental results [9,16] and fundamental understanding for elucidating the origin of the interactions that are at the basis of the predicted structures. We find that counteracting vacancy-induced lattice relaxation effects of neighboring vacancies—which are intimately related to the excess-charge localization phenomena—leading to repulsive vacancy interactions, is essential to the predicted preferred vacancy spacing equal to twice the (1×1) surface lattice constant. Our results bring the long-standing puzzle concerning the structure of the reduced CeO_2 surface closer to a solution.

Generally speaking, the geometric and electronic structure of oxygen vacancies in reducible oxides and their interactions is of continued interest in surface science and of great importance for established and emerging technologies. Fundamental understanding of such defects is paramount for exploiting the interplay between structure and electronic and ionic processes and reactivity. Recently, surface oxygen vacancies were (also) found to be less stable than those in deeper layers for the TiO_2 anatase (101) surface [34]. Clearly, the oxygen vacancy stability cannot be ignored when considering the surface physics and chemistry of reducible oxides; thus, earlier data may need to be reinterpreted. We think that there is room for surprise, considering that the surface chemistry of such oxides is often defect driven.

We thank EULANEST (042-CERENH2/MINECO-PIM2010EEUU00138), MINECO (CTQ2012-32928), and CONICET (PIP-0258, PIP-0038) for financial support. Computer time provided by the SGAI-CSIC, CESGA, BSC, and BIFI-ZCAM is thankfully acknowledged. We thank Javier Carrasco for stimulating discussions and Oscar Custance, Michael Reichling, and Geoff Thornton for details on their experimental results. The COST Action CM1104 is gratefully acknowledged.

*Corresponding author.
vgp@icp.csic.es

[1] M. S. Dresselhaus and I. L. Thomas, Nature (London) **414**, 332 (2001).
[2] Q. Fu, H. Saltsburg, and M. Flytzani-Stephanopoulos, Science **301**, 935 (2003).
[3] G. A. Deluga, J. R. Salge, L. D. Schmidt, and X. E. Verykios, Science **303**, 993 (2004).
[4] J. A. Rodriguez, S. Ma, P. Liu, J. Hrbek, J. Evans, and M. Pérez, Science **318**, 1757 (2007).
[5] S. Park, J. M. Vohs, and R. J. Gorte, Nature (London) **404**, 265 (2000).
[6] C. T. Campbell and C. H. F. Peden, Science **309**, 713 (2005).
[7] Z. Dohnálek, I. Lyubinetsky, and R. Rousseau, Prog. Surf. Sci. **85**, 161 (2010).
[8] F. Esch, S. Fabris, L. Zhou, T. Montini, C. Africh, P. Fornasiero, G. Comelli, and R. Rosei, Science **309**, 752 (2005).
[9] S. Torbrügge, M. Reichling, A. Ishiyama, S. Morita, and O. Custance, Phys. Rev. Lett. **99**, 056101 (2007).
[10] M. V. Ganduglia-Pirovano, A. Hofmann, and J. Sauer, Surf. Sci. Rep. **62**, 219 (2007), and references therein.
[11] M. V. Ganduglia-Pirovano, J. L. F. Da Silva, and J. Sauer, Phys. Rev. Lett. **102**, 026101 (2009).
[12] H. Y. Li, H. F. Wang, X. Q. Gong, Y. L. Guo, Y. Guo, G. Lu, and P. Hu, Phys. Rev. B **79**, 193401 (2009).
[13] J. C. Conesa, Catal. Today **143**, 315 (2009).
[14] C. Zhang, A. Michaelides, D. A. King, and S. J. Jenkins, Phys. Rev. B **79**, 075433 (2009).
[15] M. Fronzi, A. Soon, B. Delley, E. Traversa, and C. Stampfl, J. Chem. Phys. **131**, 104701 (2009).
[16] D. C. Grinter, R. Ithnin, C. L. Pang, and G. Thorton, J. Phys. Chem. C **114**, 17036 (2010).
[17] J. F. Jerratsch, X. Shao, N. Nilius, H. J. Freund, C. Popa, M. V. Ganduglia-Pirovano, A. M. Burow, and J. Sauer, Phys. Rev. Lett. **106**, 246801 (2011).
[18] A. P. Amrute, C. Mondelli, M. Moser, G. Novell-Leruth, N. López, D. Rosenthal, R. Farra, M. E. Schuster, Teschner, T. Schmidt *et al.*, J. Catal. **286**, 287 (2012).
[19] Z. Yang, T. W. Woo, M. Baudin, and K. Hermansson, J. Chem. Phys. **120**, 7741 (2004).
[20] S. Fabris, G. Vicario, G. Balducci, S. de Gironcoli, and S. Baroni, J. Phys. Chem. B **109**, 22860 (2005).
[21] M. Nolan, S. C. Parker, and G. W. Watson, Surf. Sci. **595**, 223 (2005).
[22] J. P. Perdew, K. Burke, and M. Ernzerhof, Phys. Rev. Lett. **77**, 3865 (1996).
[23] VASP 5.2.12 (11 November 2011), http://www.vasp.at/.
[24] S. L. Dudarev, G. A. Botton, S. Y. Savrasov, C. J. Humphreys, and A. P. Sutton, Phys. Rev. B **57**, 1505 (1998).
[25] M. Cococcioni and S. de Gironcoli, Phys. Rev. B **71**, 035105 (2005).
[26] See Supplemental Material at http://link.aps.org/supplemental/10.1103/PhysRevLett.110.246101 for details.
[27] A. V. Krukau, O. A. Vydrov, A. F. Izmaylov, and G. E. Scuseria, J. Chem. Phys. **125**, 224106 (2006).
[28] K. Reuter and M. Scheffler, Phys. Rev. B **65**, 035406 (2001).
[29] M. V. Ganduglia-Pirovano and J. Sauer, Phys. Rev. B **70**, 045422 (2004).
[30] M. P. Seah, J. Phys. F **10**, 1043 (1980).
[31] J. L. F. Da Silva, M. V. Ganduglia-Pirovano, J. Sauer, V. Bayer, and G. Kresse, Phys. Rev. B **75**, 045121 (2007).
[32] E. Shoko, M. F. Smith, and R. H. McKenzie, J. Phys. Chem. Solids **72**, 1482 (2011).
[33] H. L. Tuller and A. S. Nowick, J. Phys. Chem. Solids **38**, 859 (1977).
[34] P. Scheiber, M. Fidler, O. Dulub, M. Schmid, U. Diebold, W. Hou, U. Aschauer, and A. Selloni, Phys. Rev. Lett. **109**, 136103 (2012).
[35] *CRC Handbook of Chemistry and Physics*, edited by D. R. Lide and H. P. Frederiske (CRC, Boca Raton, 1995), 76th ed.